Supplementary Material for Can molecular simulations reliably compare homogeneous and heterogeneous ice nucleation?

Dominic Atherton,[1] Angelos Michaelides,[1] and Stephen J. Cox[1]
Yusuf Hamied Department of Chemistry, University of Cambridge, Lensfield Road, Cambridge CB2 1EW, United Kingdom[a)]

(Dated: 20 April 2022)

This document includes: background theory for calculating the free energy of the liquid and crystalline phases; a detailed workflow; results obtained with the TIP4P/2005 water model; and best-fit coefficients for density vs pressure. We also present a discussion on impulsive forces.

S1. BACKGROUND THEORY FOR CALCULATING THE FREE ENERGY OF THE LIQUID AND CRYSTALLINE PHASES

To help set notation, and highlight slight differences in approach compared to previous studies, we will briefly cover some of the theory underlying the free energy calculations performed in the main article.

A. Liquid

As we consider rigid water molecules, the position of all atoms in molecule i can be specified entirely by the location of its oxygen atom $\mathbf{r}_i^{(\mathrm{O})} \equiv \mathbf{R}_i$ and its orientation $\mathbf{\Omega}_i$. The translational and rotational momentum of molecule i are denoted $\mathbf{p}_i$ and $\mathbf{L}_i$, respectively. The partition function for a system comprising N indistinguishable molecules can thus be written as

$$Q = \frac{1}{h^{6N}N!}\int \mathrm{d}\mathbf{p}^N \int \mathrm{d}\mathbf{L}^N \int \mathrm{d}\mathbf{R}^N \int \mathrm{d}\mathbf{\Omega}^N \mathrm{e}^{-\beta\mathcal{K}_\mathrm{t}(\mathbf{p}^N)}\mathrm{e}^{-\beta\mathcal{K}_\mathrm{r}(\mathbf{L}^N)}\mathrm{e}^{-\beta\mathcal{U}(\mathbf{R}^N,\mathbf{\Omega}^N)}, \tag{S1}$$

$$= \frac{(8\pi^2)^N V^N}{h^{6N}N!}\int \mathrm{d}\mathbf{p}^N\, \mathrm{e}^{-\beta\mathcal{K}_\mathrm{t}(\mathbf{p}^N)} \int \mathrm{d}\mathbf{L}^N\, \mathrm{e}^{-\beta\mathcal{K}_\mathrm{r}(\mathbf{L}^N)} \frac{1}{V^N}\int \mathrm{d}\mathbf{R}^N \frac{1}{(8\pi^2)^N}\int \mathrm{d}\mathbf{\Omega}^N \mathrm{e}^{-\beta\mathcal{U}(\mathbf{R}^N,\mathbf{\Omega}^N)}, \tag{S2}$$

where h^{6N} defines a volume element in phase space, $\mathcal{K}_\mathrm{t}$ and $\mathcal{K}_\mathrm{r}$ are the translational and rotational kinetic energy, respectively, and $\mathcal{U}$ is the potential energy. For non-linear rigid molecules like the water models considered,

$$\mathcal{K}_\mathrm{r}(\mathbf{L}) = \sum_{i=1}^{N} \frac{|\mathbf{L}_i^{(1)}|^2}{2I^{(1)}} + \frac{|\mathbf{L}_i^{(2)}|^2}{2I^{(2)}} + \frac{|\mathbf{L}_i^{(3)}|^2}{2I^{(3)}}, \tag{S3}$$

where the superscripts indicate different principal axes of rotation, and $I^{(1)}$ indicates the moment of inertia around axis 1 etc. The ideal contribution to the partition function is then

$$Q_\mathrm{id} = \frac{(8\pi^2)^N V^N}{\Lambda^{3N}N!}\left(\frac{2\pi k_\mathrm{B}TI^{(1)}}{h^2}\right)^{N/2}\left(\frac{2\pi k_\mathrm{B}TI^{(2)}}{h^2}\right)^{N/2}\left(\frac{2\pi k_\mathrm{B}TI^{(3)}}{h^2}\right)^{N/2}. \tag{S4}$$

If the total mass of a molecule is m, then we can write e.g.,

$$\left(\frac{2\pi m k_\mathrm{B}T}{h^2}\right)^{N/2}\left(\frac{I^{(1)}}{m}\right)^{N/2} = \frac{1}{\Lambda^N}\left(\frac{I^{(1)}}{m}\right)^{N/2}.$$

a)Electronic mail: sjc236@cam.ac.uk

Thus,

$$\ln Q_{\rm id} \approx N \ln\left(\frac{V}{N\Lambda^3}\right) + N$$
$$+N\ln\left[\left(\frac{I^{(1)}}{m}\right)^{1/2}\frac{1}{\Lambda}\right] + N\ln\left[\left(\frac{I^{(2)}}{m}\right)^{1/2}\frac{1}{\Lambda}\right] + N\ln\left[\left(\frac{I^{(3)}}{m}\right)^{1/2}\frac{1}{\Lambda}\right] + N\ln 8\pi^2 \tag{S5}$$
$$= -N\ln\left(\bar{\rho}\Lambda^3\right) + N - N\ln\left[\left(\frac{m^3}{I^{(1)}I^{(2)}I^{(3)}}\right)^{1/2}\frac{\Lambda^3}{8\pi^2}\right], \tag{S6}$$
$$= -N\ln\left(\bar{\rho}\eta_{\rm r}\Lambda^6\right) + N, \tag{S7}$$

where we have defined

$$\eta_{\rm r} \equiv \left(\frac{m^3}{I^{(1)}I^{(2)}I^{(3)}}\right)^{1/2}\frac{1}{8\pi^2}.$$

Let us now write $\eta_{\rm r}^{1/6}\Lambda = \bar{\Lambda}_0 T^{-1/2}$, such that $\bar{\Lambda}_0 T_0^{-1/2} = 1\,\text{Å}^{1/2}$. Then,

$$\eta_{\rm r}^{1/6}\Lambda = \bar{\Lambda}_0 T_0^{-1/2}\left(\frac{T_0}{T}\right)^{1/2} = \left(\frac{T_0}{T}\right)^{1/2}\text{Å}^{1/2}.$$

The ideal free energy can then be written as,

$$\frac{\beta A_{\rm id}}{N} = \beta a_{\rm id} = \ln\left(\bar{\rho}(T_0/T)^3\right) - 1, \tag{S8}$$

where it is understood that (T_0/T) carries units of Å. The choice of reference temperature T_0 is arbitrary provided it is chosen consistently. This approach differs from the common 'set $\Lambda = 1\,$Å' encountered in the literature.[1] By adopting this approach we use, e.g., the full enthalpy when performing thermodynamic integration (c.f. Ref. 2).

The excess part of the partition function is

$$Q_{\rm ex} = \frac{1}{(8\pi^2 V)^N}\int {\rm d}\mathbf{R}^N \int {\rm d}\mathbf{\Omega}^N {\rm e}^{-\beta\mathcal{U}(\mathbf{R}^N,\mathbf{\Omega}^N)}. \tag{S9}$$

Note that, if $\mathcal{U}$ is independent of Ω e.g., we turn off the charges in our water model, then $Q_{\rm ex}$ reduces to that of a simple mono-atomic system. This means we are free to use equations of state for the standard LJ liquid where appropriate; we make use of this fact to calculate the excess free energy of the liquid by thermodynamic integration.

B. Ice

Unlike liquid water, the molecules in the crystalline phase are distinguishable by virtue of their association with a particular set of lattice sites. This leads to a straightforward modification of the partition function:

$$Q = \frac{1}{h^{6N}}\int {\rm d}\mathbf{p}^N \int {\rm d}\mathbf{L}^N \int {\rm d}\mathbf{R}^N \int {\rm d}\mathbf{\Omega}^N {\rm e}^{-\beta\mathcal{K}_{\rm t}(\mathbf{p}^N)}{\rm e}^{-\beta\mathcal{K}_{\rm r}(\mathbf{L}^N)}{\rm e}^{-\beta\mathcal{U}(\mathbf{R}^N,\mathbf{\Omega}^N)} \tag{S10}$$

Instead of dealing with 'ideal' and 'excess' quantities, it is now useful to consider 'kinetic' and 'configurational' quantities:

$$Q_{\rm kin} = \frac{1}{\Lambda^{6N}\eta_{\rm r}^N}, \tag{S11}$$

$$Q_{\rm con} = \frac{1}{(8\pi^2)^N}\int {\rm d}\mathbf{r}_{\rm O}^N \int {\rm d}\mathbf{\Omega}^N {\rm e}^{-\beta\mathcal{U}(\mathbf{r}_{\rm O}^N,\mathbf{\Omega}^N)}. \tag{S12}$$

Note that $Q_{\rm kin}$ and $Q_{\rm con}$ have dimensions of hyperdensity and hypervolume, respectively; it is important that units are chosen consistently. The factor $1/(8\pi^2)^N$ is still included in $Q_{\rm con}$ to ensure a consistent definition of η_r. By similar reasoning to above, we can write the kinetic contribution to the free energy as

$$\frac{\beta A_{\rm kin}}{N} = \beta a_{\rm kin} = \ln\left((T_0/T)^3\right). \tag{S13}$$

As detailed below, we have used the Frenkel-Ladd approach,[3] adapted by Vega and co-workers for rigid SPC water models,[1,4,5] to calculate the difference in free energy between a non-interacting crystal with its atoms tethered to their equilibrium positions by harmonic springs, and the fully interacting crystal. The potential energy of the former, 'reference', system is

$$\mathcal{U}_{\rm ref}(\mathbf{R}^N, \mathbf{\Omega}^N) = \sum_i^N \sum_\alpha \frac{k^{(\alpha)}}{2}\left(\mathbf{R}_i + \Delta\mathbf{r}_i^{(\alpha)}(\mathbf{\Omega}_i) - \mathbf{r}_i^{(\alpha,0)}\right)^2, \tag{S14}$$

where $\Delta\mathbf{r}_i^{(\alpha)} = \mathbf{r}_i^{(\alpha)} - \mathbf{R}_i$, $\mathbf{r}_i^{(\alpha,0)}$ is the equilibrium position of atom α of molecule i (recall that $\mathbf{r}_i^{(\rm O)} \equiv \mathbf{R}_i$), and $k^{(\alpha)}$ determines the strength of the harmonic potential that tethers atom α to $\mathbf{r}_i^{(\alpha,0)}$. The rigid body constraints mean that the free energy of this reference system is analytically intractable. We therefore define a 'sub-reference' system with the following potential energy,

$$\mathcal{U}_{\rm sub}(\mathbf{R}^N) = \sum_i^N \frac{k^{(\rm O)}}{2}\left(\mathbf{r}_i^{(\rm O)} - \mathbf{r}_i^{(\rm O,0)}\right)^2. \tag{S15}$$

The configurational partition function for this sub-reference system is just that of the standard Einstein crystal,

$$Q_{\rm sub} = \int \mathrm{d}\mathbf{R}^N \exp\left(-\beta\mathcal{U}_{\rm sub}(\mathbf{R}^N)\right), \tag{S16}$$

resulting in the following free energy per particle:

$$\beta a_{\rm sub} = -\frac{3}{2}\ln\left(\frac{2\pi}{\beta k^{(\rm O)}}\right). \tag{S17}$$

S2. WORKFLOW: FREE ENERGY CALCULATIONS OF ICE I_h

The procedure described below was performed for both truncation schemes described in the main article and both water models, i.e., for TIP4P/ice$^{(8.5\to\infty)}$, TIP4P/ice$^{(8.5)}$, TIP4P/2005$^{(8.5\to\infty)}$, and TIP4P/2005$^{(8.5)}$. Unless otherwise stated, all simulations used the `LAMMPS` simulation package.[6] The particle-particle particle-mesh Ewald method was used to account for long-ranged interactions,[7] with parameters chosen such that the root mean square error in the forces were a factor 10^5 smaller than the force between two unit charges separated by a distance of 0.1 nm.[8] The geometry of the water molecules was constrained using the `RATTLE` algorithm.[9] A time step of 2 fs was used throughout.

A. Obtaining average cell parameters

A proton disordered ice I_h structure comprising 768 molecules was generated using the GenIce software package.[10] After equilibration of at least 0.5 ns, the average cell parameters were obtained from a 10 ns simulation at $p = 0$ bar and temperature $T = T_{\rm i}$, with $T_{\rm i} = 272$ K for TIP4P/ice, and $T_{\rm i} = 252$ K for TIP4P/2005. Temperature was maintained with a Nosé-Hoover chain thermostat[11,12] with a damping constant 0.2 ps, and the pressure was maintained with a Parrinello-Rahman barostat[13] with a damping constant 2 ps. The latter was applied such that all cell lengths and angles could fluctuate independently.

B. Obtaining the reference ice structure

The simulation cell parameters were fixed to their average values, and the structure was 'minimized' by running short (approximately 10-20 ps) simulations at $T = 0.1$ K. The damping constant of the Nosé-Hoover chain thermostat was reduced to 20 fs. As explained in the main text, this approach was adopted as standard minimizers available in `LAMMPS` are incompatible with the `RATTLE` algorithm used to constrain the rigid geometry of the water molecules. Simulation settings were otherwise the same as above.

C. Thermodynamic integration from the non-interacting to interacting crystal

Atoms were tethered to their positions in the reference ice structure with force constants $k^{(\mathrm{O})} = 4.8\,\mathrm{kcal/mol\text{-}Å^2}$ and $k^{(\mathrm{H})} = 6.0\,\mathrm{kcal/mol\text{-}Å^2}$ (see Sec. S1 B). For each water model and truncation scheme considered, we constructed the following potential energy function:

$$\mathcal{U}_\lambda(\mathbf{R}^N, \mathbf{\Omega}^N) = \lambda \mathcal{U}(\mathbf{R}^N, \mathbf{\Omega}^N) + (1-\lambda)\mathcal{U}_{\mathrm{ref}}(\mathbf{R}^N, \mathbf{\Omega}^N), \tag{S18}$$

where $\mathcal{U}$ is replaced with $U^{(r_\mathrm{c}\to\infty)}$ or $U^{(r_\mathrm{c})}$ as appropriate (see Eqs. 5 and 8). The Helmholtz free energy difference between the reference and interacting systems is then,

$$\Delta_{\mathrm{r2i}}a = \frac{1}{N}\int_0^1 \mathrm{d}\lambda\, \langle \Delta U(\mathbf{R}^N, \mathbf{\Omega}^N)\rangle_\lambda, \tag{S19}$$

where $\Delta U(\mathbf{R}^N, \mathbf{\Omega}^N) = \mathcal{U}(\mathbf{R}^N, \mathbf{\Omega}^N) - \mathcal{U}_{\mathrm{ref}}(\mathbf{R}^N, \mathbf{\Omega}^N)$, and $\langle\cdots\rangle_\lambda$ denotes a canonical ensemble average according to the Hamiltonian specified by $\mathcal{U}_\lambda$. The integral in Eq. S19 was evaluated using 11-point Gauss-Legendre quadrature, and simulations for each value of λ were 20 ns in length. Temperature was maintained through Langevin dynamics as implemented in `LAMMPS`,[14,15] with a damping constant 100 fs. The total random force was set exactly to zero to ensure the center-of-mass of the system did not drift.

D. Thermodynamic integration from the sub-reference to reference system

As molecules in both the sub-reference and reference systems are non-interacting, we need only consider the behavior of a single water molecule. Specifically, we construct the following energy function:

$$u_\lambda(\mathbf{R}_1, \mathbf{\Omega}_1) = \lambda \mathcal{U}_{\mathrm{ref}}^{(N=1)}(\mathbf{R}_1, \mathbf{\Omega}_1) + (1-\lambda)\mathcal{U}_{\mathrm{sub}}^{(N=1)}(\mathbf{R}_1, \mathbf{\Omega}_1), \tag{S20}$$

where $\mathcal{U}_{\mathrm{ref}}^{(N=1)}$ and $\mathcal{U}_{\mathrm{sub}}^{(N=1)}$ are given by Eqs. S14 and S15 with $N = 1$. The change in Helmholtz free energy is then given by:

$$\Delta_{\mathrm{s2r}}a = \int_0^1 \mathrm{d}\lambda\, \langle \Delta u(\mathbf{R}^N, \mathbf{\Omega}^N)\rangle_\lambda, \tag{S21}$$

with $\Delta u = \mathcal{U}_{\mathrm{ref}}^{(N=1)} - \mathcal{U}_{\mathrm{sub}}^{(N=1)}$, and $\langle\cdots\rangle_\lambda$ now denotes a canonical ensemble average at temperature T_i according to the Hamiltonian specified by u_λ. The integral in Eq. S21 was again evaluated using 11-point Gauss-Legendre quadrature, using a bespoke Metropolis Monte Carlo (MC) code. In brief, after 10^4 MC moves for equilibration, production simulations of 5×10^7 MC moves were performed for each value of λ. For each MC move, the water molecule was either translated or rotated with equal probability. For translations, a displacement along each Cartesian direction was randomly chosen in the interval $[-\sqrt{2/\beta k^{(\mathrm{O})}}, \sqrt{2/\beta k^{(\mathrm{O})}})$. For rotations, three angles (α, β, γ) were randomly chosen in the interval $[0, \pi/6)$, and a rotation matrix was constructed as $\mathbf{R} = \mathbf{R}_z(\alpha)\mathbf{R}_y(\beta)\mathbf{R}_x(\gamma)$, where $\mathbf{R}_x(\gamma)$ is a rotation about the x-axis etc. With equal probability, the molecule was then rotated about its oxygen position using either $\mathbf{R}$ or its transpose. Note that, as $\Delta_{\mathrm{s2r}}a$ is independent of truncation scheme, we only computed it once for each water model.

E. Computing $\beta\mu_{\mathrm{ice}}(T)$

With an estimate of $\beta_\mathrm{i}\mu_{\mathrm{ice}}(T_\mathrm{i})$ obtained from thermodynamic integration, $\beta\mu_{\mathrm{ice}}(T)$ is computed from the Gibbs-Helmholtz relation (Eq. 12). For TIP4P/ice$^{(8.5\to\infty)}$ and TIP4P/ice$^{(8.5)}$, simulations in the temperature range $T = 267\,\mathrm{K}, 268\,\mathrm{K}, \ldots, 277\,\mathrm{K}$, and $T = 267\,\mathrm{K}, 268\,\mathrm{K}, \ldots, 282\,\mathrm{K}$, respectively, were performed, while for TIP4P/2005$^{(8.5\to\infty)}$ and TIP4P/2005$^{(8.5)}$ we adopted the temperature range $T = 247\,\mathrm{K}, 248\,\mathrm{K}, \ldots, 267\,\mathrm{K}$. Simulations were initialized from the reference structure, starting at 0.1 K with the temperature steadily increased to T over 1 ns at constant volume. An equilibration period of 0.5 ns at constant T and $p = 0\,\mathrm{bar}$ was then performed (see Sec. S2 A), followed by a production run of 20 ns. The integrand in Eq. 12 was then fitted to a quadratic polynomial, from which $\beta\mu_{\mathrm{ice}}(T)$ was obtained by analytic integration.

S3. WORKFLOW: FREE ENERGY CALCULATIONS OF LIQUID WATER

The procedure described below is again appropriate for both truncation schemes and both water models. Simulation details were broadly similar to those specified throughout Sec. S2.

A. Obtaining the average density of liquid water

A 20 ns simulation of liquid water was performed after at least 0.5 ns equilibration at temperature T_i and $p = 0$ bar. A Nosé-Hoover chain thermostat was used to maintain the temperature, and an isotropic Parrinello-Rahman barostat was used to maintain the pressure.

B. Thermodynamic integration from the LJ fluid to water

To compute the excess free energy of liquid water, we exploit the fact that the equation of state for the LJ fluid has been computed previously, which provides $a_{\mathrm{LJ,ex}}^{(r_\mathrm{c}\to\infty)}$. The density of the fluid is fixed to its average (see Sec. S3 A) at temperature T_i and $p = 0$ bar, and thermodynamic integration is performed with the following energy function:

$$\mathcal{U}_\lambda(\mathbf{R}^N, \mathbf{\Omega}^N) = \mathcal{U}(\mathbf{R}^N, \mathbf{\Omega}^N) \text{ with charges multiplied by } \lambda^{1/2}. \tag{S22}$$

(We reuse the notation $\mathcal{U}_\lambda$ as it should be clear from context what is intended.) Again, $\mathcal{U}$ is replaced with $U^{(r_\mathrm{c}\to\infty)}$ or $U^{(r_\mathrm{c})}$ as appropriate. The free energy difference $\Delta_{\mathrm{LJ2w}}a$ between water and the LJ fluid is then given by an expression analogous to Eq. S19, with the integral evaluated by 9-point Gauss-Legendre quadrature. For each value of λ, $\langle \Delta U(\mathbf{R}^N, \mathbf{\Omega}^N)\rangle_\lambda$ was averaged over a 20 ns simulation, following a 0.5 ns equilibration period.

C. Thermodynamic integration from the 'truncated + tail corrections' LJ fluid to 'cut-and-shift' LJ fluid

For systems employing the 'cut-and-shift' truncation scheme, we also computed the free energy difference between the fluid with interactions described by $u_{\mathrm{LJ}}^{(r_\mathrm{c}\to\infty)}$ and $u_{\mathrm{LJ}}^{(r_\mathrm{c})}$. As dynamics in the canonical ensemble are unaffected by this choice of truncation scheme, we simply have (see Eq. S22)

$$\Delta_{\mathrm{tc2cs}}a = \left\langle U_{\lambda=0}^{(8.5)}(\mathbf{R}^N, \mathbf{\Omega}^N) - U_{\lambda=0}^{(8.5\to\infty)}(\mathbf{R}^N, \mathbf{\Omega}^N)\right\rangle, \tag{S23}$$

which we calculated from a 20 ns simulation, following a 0.5 ns equilibration period.

D. Computing $\beta\mu_{\mathrm{liq}}(T)$

Using the same temperature ranges described in Sec. S2 E, the Gibbs-Helmholtz equation was evaluated in an analogous manner to $\beta\mu_{\mathrm{ice}}(T)$. For each temperature, a 0.5 ns equilibration period was performed followed by a 20 ns production run. The pressure was maintained with an isotropic barostat (see Sec. S3 A).

S4. WORKFLOW: LOCATING THE MELTING POINT

For each water model and truncation scheme, $\beta\mu_{\mathrm{ice}}(T)$ and $\beta\mu_{\mathrm{liq}}(T)$ were each fitted to a quadratic polynomial, and the melting temperature was obtained by solving the resulting simultaneous equations.

S5. WORKFLOW: HAMILTONIAN GIBBS-DUHEM INTEGRATION

With $T_\mathrm{m}^{(8.5)}$ determined from the free energy approach described above, $T_\mathrm{m}^{(9.25)}$ and $T_\mathrm{m}^{(10.0)}$ were subsequently determined by Hamiltonian Gibbs-Duhem integration. Specifically, we define the potential energy function

$$U_\lambda(\mathbf{R}^N, \mathbf{\Omega}^N) = \lambda U^{(r_{\mathrm{c},1})}(\mathbf{R}^N, \mathbf{\Omega}^N) + (1-\lambda)U^{(r_{\mathrm{c},0})}(\mathbf{R}^N, \mathbf{\Omega}^N), \tag{S24}$$

and the quantity,

$$x_\alpha^{(\lambda)} = \frac{1}{N}\left\langle U^{(r_{\mathrm{c},1})}(\mathbf{R}^N, \mathbf{\Omega}^N) - U^{(r_{\mathrm{c},0})}(\mathbf{R}^N, \mathbf{\Omega}^N)\right\rangle_\lambda, \tag{S25}$$

where α indicates sampling of the ice or liquid phase. The derivative of the melting temperature with respect to λ is then

$$\frac{\mathrm{d}T_\mathrm{m}^{(r_{\mathrm{c},\lambda})}}{\mathrm{d}\lambda} = \frac{T\left(x_\mathrm{ice}^{(\lambda)} - x_\mathrm{liq}^{(\lambda)}\right)}{h_\mathrm{ice}^{(\lambda)} - h_\mathrm{liq}^{(\lambda)}}, \tag{S26}$$

where $h_\mathrm{ice}^{(\lambda)}$ and $h_\mathrm{liq}^{(\lambda)}$ are the enthalpies per particle of ice and liquid, respectively, obtained from trajectories using U_λ. Starting from $T_\mathrm{m}^{(8.5)}$, $T_\mathrm{m}^{(9.25)}$ was obtained by integrating Eq. S26 by fourth-order Runge-Kutta integration. This was then repeated, starting from $T_\mathrm{m}^{(9.25)}$, to obtain an estimate for $T_\mathrm{m}^{(10.0)}$. We implemented U_λ by tabulating the potential at 0.0005 Å intervals for $1.8\,\text{Å} < r < 10.1\,\text{Å}$, but otherwise, simulation settings were the same as those described in Secs. S2 A and S3 A. Simulations were 5 ns, following 0.5 ns equilibration.

S6. WORKFLOW: LIQUID-VAPOR SIMULATIONS

Simulations to produce Figs. 3b and S1b comprised 512 water molecules, using TIP4P/ice and TIP4P/2005, respectively. Simulation details are broadly similar to those described in S3. The cross sectional (xy) area of the simulation box was $19.7 \times 19.7\,\text{Å}^2$, and its length normal (z) to the liquid-vapor interface was 90 Å. To facilitate post-processing analysis, repulsive walls as described in Ref. 16 were placed at the edges of the simulation cell along z to prevent molecules escaping the primary simulation cell. The electric displacement field along z was set to zero, using the implementation given in Refs. 17 and 18; this is formally equivalent to the commonly used slab correction of Yeh and Berkowitz.[19] Production simulations were performed for 20 ns following at least 0.5 ns equilibration. A Nosé-Hoover chain thermostat was used to maintain the temperature at 300 K. 'Tail corrections' were formally applied, but as discussed in the main text, this produces the same dynamics as the 'cut-and-shift' potential.

S7. RESULTS FOR TIP4P/2005

In this section, we present results obtained with TIP4P/2005. While quantitative differences are expected, and indeed observed, our general conclusions are unaffected by the choice of water model. At $p = 0$ bar, we find $T_\mathrm{m}^{(8.5\to\infty)} = 251.9$ K in good agreement with $T_\mathrm{m} = 252 \pm 6$ K reported previously for $p = 1$ bar. We also see a modest increase in melting temperature when using TIP4P/2005$^{(8.5)}$, with $T_\mathrm{m}^{(8.5)} = 253.4$ K and $T_\mathrm{m}^{(\mathrm{MF},8.5)} = 254.0$ K. The predictions of the mean-field prediction are supported by Hamiltonian Gibbs-Duhem integration. Note that, unlike the results for TIP4P/ice$^{(r_\mathrm{c})}$ reported in the main paper (Fig. 5b), the Hamiltonian Gibbs-Duhem simulations performed for TIP4P/2005$^{(r_\mathrm{c})}$ were initiated from $T_\mathrm{m}^{(\mathrm{MF},8.5)}$ instead of $T_\mathrm{m}^{(8.5)}$ (indicated by the blue star in Fig. S4).

S8. FITTING COEFFICIENTS

In this section, we report the coefficients for the quadratic polynomial $r_2p^2 + r_1p + r_0$ obtained using `numpy`'s `polyfit` routine,[20] as shown in Figs. 3 and 5 in the main article, and Figs. S1 and S3.

A. Results for TIP4P/ice

- Liquid, 300 K (Fig. 3a):

  $r_2 = -3.822428 \times 10^{-9}\,\mathrm{g/(bar^2\,cm^3)}$;
  $r_1 = 4.460206 \times 10^{-5}\,\mathrm{g/(bar\,cm^3)}$;
  $r_0 = 9.939254 \times 10^{-1}\,\mathrm{g/cm^3}$.

- Liquid, 272 K (Fig. 5a):

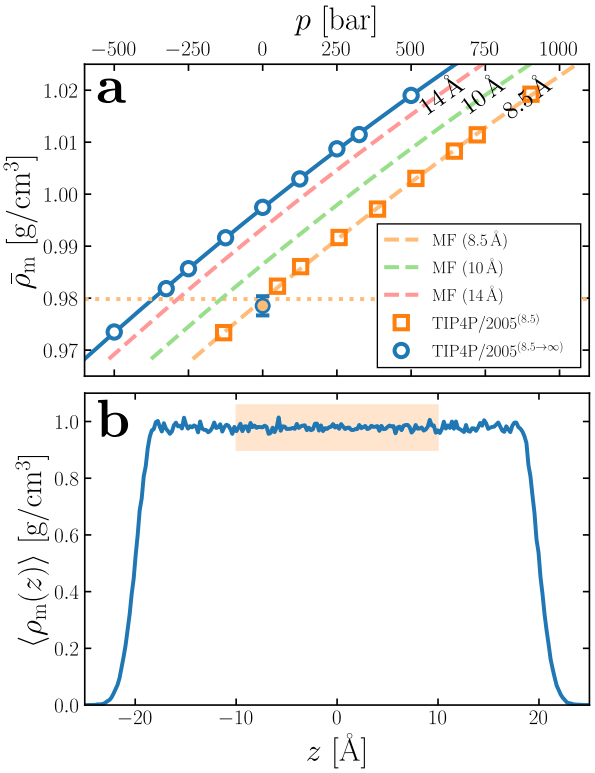

FIG. S1. Evaluating the impact of r_c on $\bar{\rho}_m$ for liquid TIP4P/2005 at 300 K. (a) $\bar{\rho}_m(p)$ for a homogeneous system. White-filled circles show results from constant-p simulations of TIP4P/2005$^{(8.5\to\infty)}$, and the solid blue line indicates a quadratic fit. Dashed lines indicate MF predictions (Eq. 9) for different r_c, as indicated in the legend. Orange squares show results from constant-p simulations of TIP4P/2005$^{(8.5)}$. The dotted line indicates $\bar{\rho}_m(0)$ for TIP4P/2005$^{(8.5)}$, which intercepts the TIP4P/2005$^{(8.5\to\infty)}$ results at $p \approx -370$ bar. (b) $\langle\rho_m(z)\rangle$ for a film of TIP4P/2005$^{(8.5\to\infty)}$ in contact with its vapor (only part of the simulation cell is shown). Spatially averaging $\langle\rho_m(z)\rangle$ in the slab's interior, as indicated by the shaded region, gives an estimate $\bar{\rho}_m(0)$, which is plotted with the orange-filled circle in (a).

$$r_2 = -4.700729 \times 10^{-9}\,\mathrm{g/(bar^2\,cm^3)};$$
$$r_1 = 5.129812 \times 10^{-5}\,\mathrm{g/(bar\,cm^3)};$$
$$r_0 = 9.898901 \times 10^{-1}\,\mathrm{g/cm^3}.$$

- Ice, 272 K (Fig. 5b):

$$r_2 = 1.442316 \times 10^{-11}\,\mathrm{g/(bar^2\,cm^3)};$$
$$r_1 = 8.358199 \times 10^{-6}\,\mathrm{g/(bar\,cm^3)};$$
$$r_0 = 9.056778 \times 10^{-1}\,\mathrm{g/cm^3}.$$

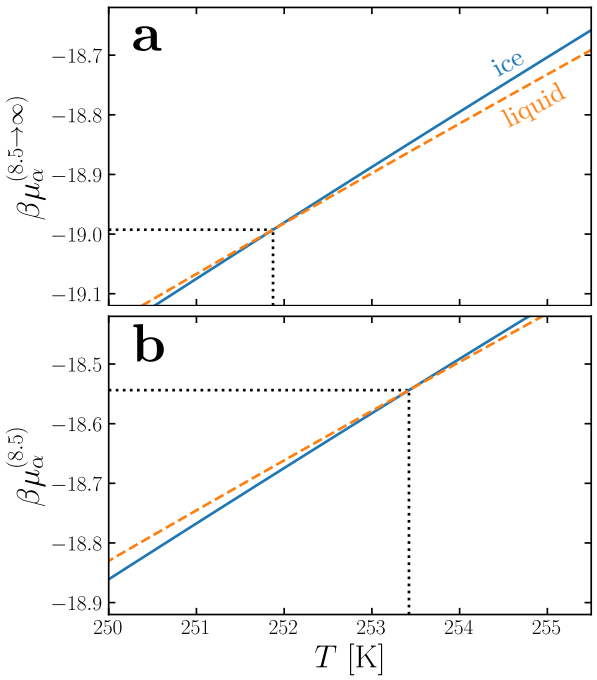

FIG. S2. $\beta\mu_\alpha(T)$ at 0 bar, with $\alpha =$ 'ice' or 'liq', for (a) TIP4P/2005$^{(8.5\to\infty)}$ and (b) TIP4P/2005$^{(8.5)}$. T_m is determined from the point of interception, as indicated by the black dotted lines, with $T_\mathrm{m}^{(8.5\to\infty)} = 251.9\,\mathrm{K}$ and $T_\mathrm{m}^{(8.5)} = 253.4\,\mathrm{K}$.

B. Results for TIP4P/2005

- Liquid, 300 K (Fig. S1a):

  $r_2 = -4.748523 \times 10^{-9}\,\mathrm{g/(bar^2\,cm^3)}$;
  $r_1 = 4.561509 \times 10^{-5}\,\mathrm{g/(bar\,cm^3)}$;
  $r_0 = 9.973669 \times 10^{-1}\,\mathrm{g/cm^3}$.

- Liquid, 252 K (Fig. S3a):

  $r_2 = -3.051495 \times 10^{-9}\,\mathrm{g/(bar^2\,cm^3)}$;
  $r_1 = 5.587068 \times 10^{-5}\,\mathrm{g/(bar\,cm^3)}$;
  $r_0 = 9.967701 \times 10^{-1}\,\mathrm{g/cm^3}$.

- Ice, 252 K (Fig. S3b):

  $r_2 = -2.226744 \times 10^{-10}\,\mathrm{g/(bar^2\,cm^3)}$;
  $r_1 = 9.123390 \times 10^{-6}\,\mathrm{g/(bar\,cm^3)}$;
  $r_0 = 9.201753 \times 10^{-1}\,\mathrm{g/cm^3}$.

S9. COMMENT ON THE APPARENT ROLE OF IMPULSIVE FORCES

We have remarked in the main article that in the canoncial ensemble, dynamics are unaffected by the choice of $U^{(r_\mathrm{c})}$ vs. $U^{(r_\mathrm{c}\to\infty)}$. While we have verified this directly by comparing trajectories, and by checking the forces between a pair of LJ particles (as implemented in `LAMMPS`), the form of $u_\mathrm{LJ}^{(r_\mathrm{c}\to\infty)}$ given by Eq. 3 suggests the presence of an impulsive force at $r = r_\mathrm{c}$. Here will we demonstrate that including impulsive forces would be inconsistent with standard implementations of tail corrections.

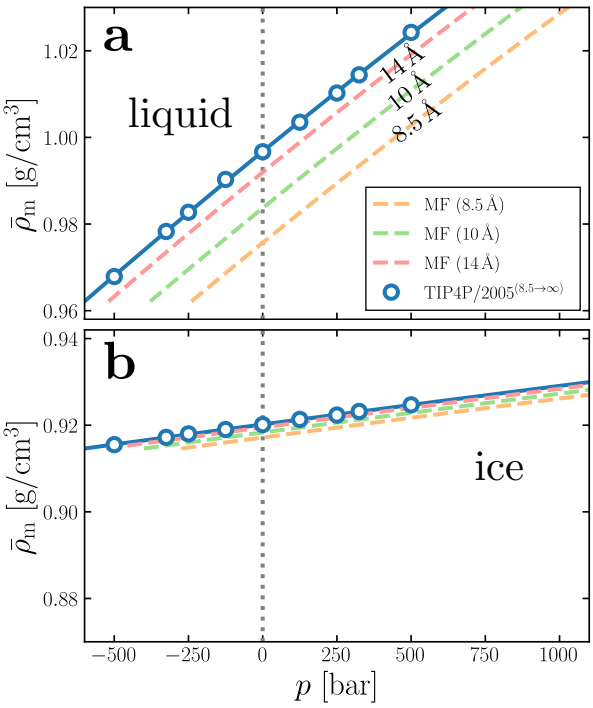

FIG. S3. $\bar{\rho}_m(p)$ at 252 K for (a) liquid water and (b) ice. White-filled circles show results from constant-p simulations of TIP4P/2005$^{(8.5\to\infty)}$, and the solid blue line indicates a quadratic fit. Dashed lines indicate MF predictions (Eq. 9) for different r_c, as indicated in the legend, which are used to predict $\bar{\rho}_m(0)$ for a given r_c, i.e., where the dashed lines intersect the vertical gray dotted line.

Let us introduce a system with the following potential energy:

$$U^{(r_c!)}(\mathbf{R}^N) = \sum_{i<j}^{N} u_{LJ}^{(r_c!)}(|\mathbf{r}_{ij}^{(O)}|) + U_{elec}(\mathbf{R}^N), \tag{S27}$$

with

$$u_{LJ}^{(r_c!)}(r) = u_{LJ}^{(\infty)}(r)h(r_c - r), \tag{S28}$$

where $h(r)$ is the Heaviside step function. The potential energy function $U^{(r_c!)}$ describes a system where LJ interactions are described by the unshifted LJ potential for $r \le r_c$, and abruptly vanish for $r > r_c$. Forces due to the LJ interactions are obtained by differentiation,

$$f_{LJ}^{(r_c!)}(r) = f_{LJ}^{(\infty)}(r)h(r_c - r) + u_{LJ}^{(\infty)}(r)\delta(r_c - r). \tag{S29}$$

We clearly see an impulsive force at $r = r_c$. Now consider the average virial pressure:

$$p^{(r_c!)} = \frac{2\pi\bar{\rho}^2}{3}\int_0^{r_c} \mathrm{d}r\, r^3 f_{LJ}^{(\infty)}(r) g_{OO}(r) + \frac{2\pi\bar{\rho}^2}{3} r_c^3 u_{LJ}^{(\infty)}(r_c), \tag{S30}$$

$$= \frac{2\pi\bar{\rho}^2}{3}\int_0^{r_c} \mathrm{d}r\, r^3 f_{LJ}^{(\infty)}(r) g_{OO}(r) + \frac{8\pi\epsilon\bar{\rho}^2\sigma^3}{3}\left[\left(\frac{\sigma}{r_c}\right)^9 - \left(\frac{\sigma}{r_c}\right)^3\right], \tag{S31}$$

where we have assumed that $g_{OO}(r \ge r_c) = 1$. The second term in Eq. S31, which we will denote $\Delta p^{(r_c!)}$, is the impulsive contribution to the virial. For a system where impulsive forces are present (whose dynamics in the NVT ensemble in principle differ from $U^{(r_c)}$ and $U^{(r_c\to\infty)}$ systems), one is required to add $\Delta p^{(r_c!)}$ to the virial pressure, which in turn will affect the dynamics in the NpT ensemble. If we attempt to account for neglected interactions beyond the cutoff in the usual fashion by simply adding the contribution

$$\Delta_{MF} p(r_c) = \frac{2\pi\bar{\rho}^2}{3}\int_{r_c}^{\infty} \mathrm{d}r\, r^3 f_{LJ}^{(\infty)}(r) = \frac{32\pi\epsilon\bar{\rho}^2\sigma^3}{9}\left[\left(\frac{\sigma}{r_c}\right)^9 - \frac{3}{2}\left(\frac{\sigma}{r_c}\right)^3\right] \tag{S32}$$

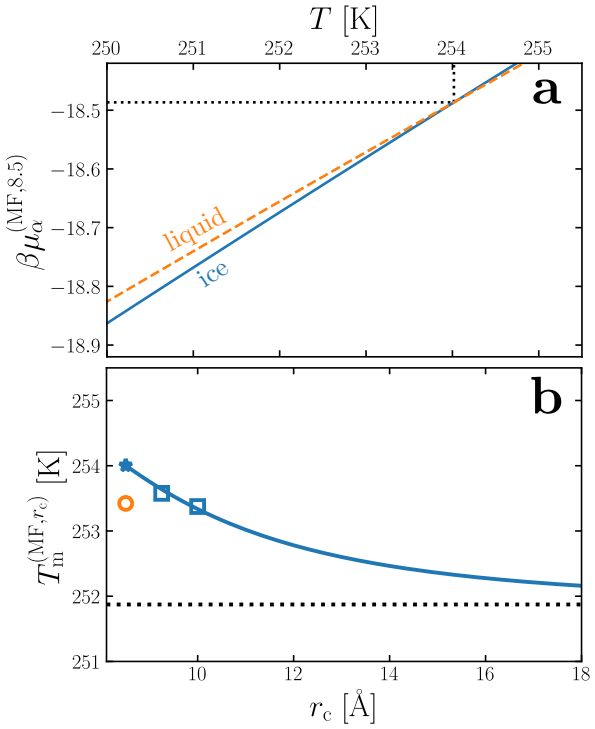

FIG. S4. Predicting the effect of r_c on the melting temperature of TIP4P/2005 with MF theory. (a) $\beta\mu_\alpha^{(\mathrm{MF},8.5)}(T)$ at $p = 0\,\mathrm{bar}$, with $\alpha =$ 'ice' or 'liq', obtained from Eq. 15. $T_\mathrm{m}^{(\mathrm{MF},8.5)} = 254.0\,\mathrm{K}$ is determined from the point of interception, as indicated by the black dotted lines. (b) $T_\mathrm{m}^{(\mathrm{MF},r_c)}$ is shown by the solid blue line. The orange circle indicates $T_\mathrm{m}^{(8.5)}$ obtained from the free energy calculations described in Sec. II, and the blue squares indicate $T_\mathrm{m}^{(9.25)}$ and $T_\mathrm{m}^{(10.0)}$ obtained from Hamiltonian Gibbs-Duhem integration, starting from $T_\mathrm{m}^{(\mathrm{MF},8.5)}$, which is marked with the blue star.

to $p^{(r_c!)}$, we find an average virial pressure,

$$\frac{2\pi\bar{\rho}^2}{3}\int_0^{r_\mathrm{c}} \mathrm{d}r\, r^3 f_\mathrm{LJ}^{(\infty)}(r) g_\mathrm{OO}(r) + \Delta p^{(r_c!)} + \Delta_\mathrm{MF} p(r_\mathrm{c}), \tag{S33}$$

that does not approximately describe the average virial pressure of a $U^{(\infty)}$ system.

Now consider a $U^{(r_c\to\infty)}$ system. The LJ pair potential is

$$u_\mathrm{LJ}^{(r_c\to\infty)}(r) = u_\mathrm{LJ}^{(\infty)}(r)h(r_\mathrm{c} - r) + u_\mathrm{LJ}^{(\infty)}(r)h(r - r_\mathrm{c}), \tag{S34}$$

with the proviso that interactions for $r > r_\mathrm{c}$ are evaluated in a mean field fashion. The forces are:

$$f_\mathrm{LJ}^{(r_c\to\infty)}(r) = f_\mathrm{LJ}^{(\infty)}(r)h(r_\mathrm{c} - r) + f_\mathrm{LJ}^{(\infty)}(r)h(r - r_\mathrm{c}) + u_\mathrm{LJ}^{(\infty)}(r)\delta(r_\mathrm{c} - r) - u_\mathrm{LJ}^{(\infty)}(r)\delta(r - r_\mathrm{c}). \tag{S35}$$

The impulsive forces at $r = r_\mathrm{c}$ cancel. Again, we consider the average virial pressure:

$$p^{(r_c\to\infty)} = \frac{2\pi\bar{\rho}^2}{3}\int_0^{r_\mathrm{c}} \mathrm{d}r\, r^3 f_\mathrm{LJ}^{(\infty)}(r) g_\mathrm{OO}(r) + \Delta p^{(r_c!)} - \Delta p^{(r_c!)} + \Delta_\mathrm{MF} p(r_\mathrm{c}), \tag{S36}$$

$$= \frac{2\pi\bar{\rho}^2}{3}\int_0^{r_\mathrm{c}} \mathrm{d}r\, r^3 f_\mathrm{LJ}^{(\infty)}(r) g_\mathrm{OO}(r) + \Delta_\mathrm{MF} p(r_\mathrm{c}). \tag{S37}$$

Equation S37 demonstrates that the standard 'tail correction,' $\Delta_\mathrm{MF}p$, is appropriate for a system that employs $u_\mathrm{LJ}^{(r_c\to\infty)}(r)$ (Eq. 3) to describe explicit LJ interactions for $r \le r_\mathrm{c}$ in which the apparent impulsive force at $r = r_\mathrm{c}$ is not included. In this case, dynamics in the $U^{(r_c\to\infty)}$ and $U^{(r_c)}$ systems are identical in the NVT ensemble. It would be inconsistent to use $\Delta_\mathrm{MF}p(r_\mathrm{c})$ in combination with a system whose dynamics includes impulsive forces (see S33).

[1] C. Vega, E. Sanz, J. Abascal, and E. Noya, J. Phys.: Condens. Matter **20**, 153101 (2008).

[2]A. Reinhardt, J. Chem. Phys. **151**, 064505 (2019).
[3]D. Frenkel and A. J. Ladd, J. Chem. Phys. **81**, 3188 (1984).
[4]E. G. Noya, M. Conde, and C. Vega, J. Chem. Phys. **129**, 104704 (2008).
[5]J. Aragones, E. G. Noya, C. Valeriani, and C. Vega, J. Chem. Phys. **139**, 034104 (2013).
[6]S. Plimpton, J. Comput. Phys. **117**, 1 (1995).
[7]R. W. Hockney and J. W. Eastwood, *Computer simulation using particles* (CRC Press, 1988).
[8]J. Kolafa and J. W. Perram, Mol. Sim. **9**, 351 (1992).
[9]H. C. Andersen, J. Comput. Phys. **52**, 24 (1983).
[10]M. Matsumoto, T. Yagasaki, and H. Tanaka, J. Comput. Chem. **39**, 61 (2018).
[11]W. Shinoda, M. Shiga, and M. Mikami, Phys. Rev. B **69**, 134103 (2004).
[12]M. E. Tuckerman, J. Alejandre, R. López-Rendón, A. L. Jochim, and G. J. Martyna, J. Phys. A **39**, 5629 (2006).
[13]M. Parrinello and A. Rahman, J. Appl. Phys. **52**, 7182 (1981).
[14]B. Dünweg and W. Paul, Int. J. Mod. Phys. C **2**, 817 (1991).
[15]T. Schneider and E. Stoll, Phy. Rev. B **17**, 1302 (1978).
[16]S. J. Cox, Proc. Natl. Acad. Sci. USA **117**, 19746 (2020).
[17]S. J. Cox and M. Sprik, J. Chem. Phys. **151**, 064506 (2019).
[18]T. Sayer and S. J. Cox, Phys. Chem. Chem. Phys. **21**, 14546 (2019).
[19]I.-C. Yeh and M. L. Berkowitz, J. Chem. Phys. **111**, 3155 (1999).
[20]C. R. Harris, K. J. Millman, S. J. van der Walt, R. Gommers, P. Virtanen, D. Cournapeau, E. Wieser, J. Taylor, S. Berg, N. J. Smith, *et al.*, Nature **585**, 357 (2020).